



Impact of plasma induced damage on the fabrication of 3D NAND flash memory

Tobias Reiter^{a,*}, Xaver Klemenschts^a, Lado Filipovic^a

^a Institute for Microelectronics, TU Wien, Gußhausstraße 27-29/E360, 1040 Vienna, Austria

ARTICLE INFO

Keywords:

Plasma Etching
Plasma-Induced Damage
Process Simulation
Selective Epitaxial Growth
3D NAND

ABSTRACT

A physical process model for dry plasma etching is presented and applied to simulate vertical channel hole etching, a critical fabrication step in modern three-dimensional (3D) NAND flash memory. The presence of physical etching with high energy ions is shown to induce damage in the underlying silicon, which results in the formation of voids during the subsequent selective epitaxial growth (SEG) step. In this manuscript, we present a model for ion induced damage by storing it as a surface property during the plasma etching simulation. A specialized advection algorithm is subsequently applied to simulate silicon SEG on the bottom source line. The model clearly shows the damage caused by the high energy particles, on the crystal nature of silicon, resulting in poor coverage during the SEG step. The removal of this damaged layer using lower energy plasmas results in highly crystalline epitaxially grown silicon. The simulation results show excellent agreement with experiments in the formation of undesired voids without the low-energy pre-epitaxial plasma treatment.

1. Introduction

Modern three-dimensional (3D) flash memory (NAND) [1,2] employs a large number of stacked control gates and insulating layers - comprised of alternating metallic (usually tungsten) and silicon dioxide (SiO_2) thin films, leading to a recent increase in storage size up to 1.33 TB [3] on a single die [4]. The fabrication of these stacks relies on using silicon nitride (Si_3N_4) as a sacrificial layer, which is etched away and replaced by tungsten in a later processing step [5]. Therefore, when the channel is being etched, the etching proceeds through a stack of alternating SiO_2 and Si_3N_4 thin layers. Until now, etching through 128 layers was possible, while anything beyond that becomes a problem for presently-available plasma etching techniques [6]. This rapid scaling drives new challenges in the etching of these stacks in order to meet the demands of further increasing memory capacity by introducing even more stacked layers, thereby dramatically increasing aspect-ratios of the feature sizes. The high aspect ratios (HARs) and small feature sizes result in the increase in the plasma densities, which also makes the process more prone to fabrication-induced damage. Due to the different framework requirements for modeling topography motion and plasma induced damage (PID) during a sequence of fabrication steps, a combined study of these two effects was not previously available. In this work we present, for the first time, a process simulation methodology

which is able to store PID effects after a topography plasma etching simulation, which is then applied in subsequent simulation steps, such as selective epitaxy. The developed method shows qualitative agreements with experimental values.

1.1. Plasma Induced Damage

Fabrication using plasma processes, such as ion-enhanced etching, play a significant role in today's advanced technologies. They have been developed to fabricate very fine patterns with anisotropic features in metal oxide semiconductor field effect transistors (MOSFETs). As the transistors and features scaled down over time, the plasma density required increasing. While advancements have been made to improve plasma processing, there is nevertheless material degradation associated with it, usually referred to as plasma-induced damage (PID) [7,8].

PID has been widely studied in silicon-based electronic devices [9]. The degradation induced by plasmas is generally categorized into three types, namely, physical, charging, and radiation damage [10]. In MOSFETs, the physical damage is induced by high-energy ion bombardment on silicon substrates or other surfaces [11]. Charging damage is induced by the current from a plasma flowing into the insulator or dielectric material [12], while radiation damage corresponds to the breaking of bonds in a material due to high-energy photon

* Corresponding author.

E-mail address: reiter@iue.tuwien.ac.at (T. Reiter).

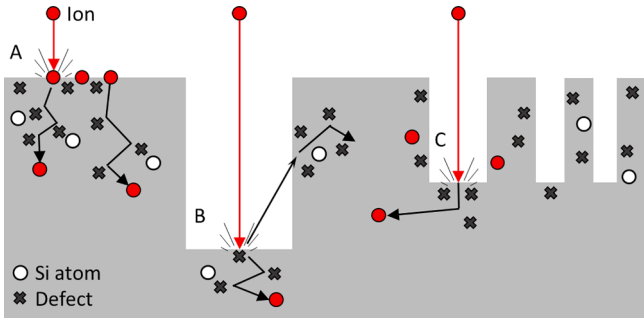


Fig. 1. Visual depiction of the physical PID mechanism in silicon based devices during plasma processing, showing (A) typical physical damage, (B) Sputtering, and (C) Lateral straggling.

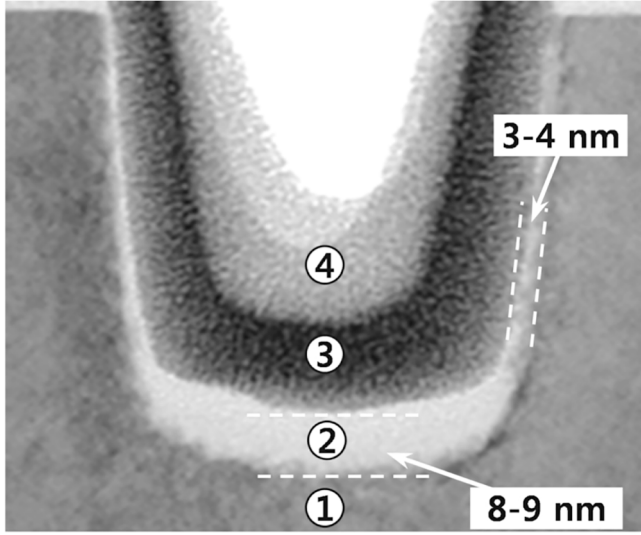


Fig. 2. TEM Micrograph [14] of the channel hole bottom after plasma etching and subsequent wet clean step. (1) Silicon substrate, (2) damaged layer, (3) tungsten, and (4) sidewall (Republished with permission of IOP Publishing, Ltd, from Luo et al., “An effective process to remove etch damage prior to selective epitaxial growth in 3D NAND flash memory”, Semiconductor Science and Technology 34, Institute of Physics (Great Britain), 2019; permission conveyed through Copyright Clearance Center, Inc.).

interactions [13]. The most relevant source of damage for the devices of interest in this manuscript, namely 3D NAND, is physical PID, which is visually represented in Fig. 1. From the figure, it can be observed that one of the damaging aspects of the process is that the crystalline nature of silicon is disrupted near the region of ion impact.

1.2. Physical PID in 3D NAND

The specific challenge in NAND fabrication is the dry etching of high-aspect-ratio vertical channel holes through the stacked $\text{SiO}_2/\text{Si}_3\text{N}_4$ layers using high energy plasmas. As previously mentioned, these types of plasma etch chemistries introduce damage in the silicon layers by implanting ions in the crystalline silicon substrate which forms the source line [11]. The physical PID leads to the introduction of a damaged layer, several nm in thickness, with a severe disorder in the crystal structure, as shown in Fig. 2, resulting in poly-crystalline selective epitaxial silicon growth (SEG). This leads to undesirable electrical properties in the source line due to the poor crystal quality, as well as the inclusion of voids in the grown silicon. Recent studies have shown that removing the damaged silicon layer using a post etch plasma treatment can effectively remove these impurities, leading to highly crystalline

SEG of silicon at the bottom [14,15].

We propose a physical model which is capable of simulating the channel hole dry etch process, including the resulting source material damage through ion implantation in a high energy plasma, leading to voids in the source contact after SEG. We show how storing the damage information on surface points and including an exponential attenuation parameter during propagation of the surface, leads to results which show excellent qualitative agreement with experimental studies. The model uses an in-house developed level set powered topography simulator ViennaLS [16] in combination with top-down Monte Carlo (MC) ray tracing provided by ViennaRay [16] to accurately describe the surface kinetics during the etching process. For the simulation of SEG, a specialized advection algorithm developed by Toifl et al. [17] is applied. The simulation tools account for multiple material regions in 3D geometries and are combined and implemented in the ViennaTools software ecosystem [16].

This manuscript is organized as follows. In Section 2 the physical process model is introduced, starting with a general explanation of level set-based surface descriptions and how the evolution of these surfaces is modeled. Subsequently, flux calculations using Monte Carlo ray tracing are described as applied for the modeling of surface kinetics and the ion-induced damage of the substrate. Finally, the model and specialized advection algorithm for the description of SEG is discussed. Section 3 shortly introduces the plasma chemistry which determines our various model parameters, after which the simulation setup is described in Section 4. The obtained results are presented in Section 5 and a conclusion is provided in Section 6.

2. Model

2.1. The Level Set Method

To accurately represent the substrate surface and its time evolution during the etching process, a level set based description is used [18]. With this method, the surface is described implicitly by a level set function $\phi(\vec{x})$ which is defined at every point \vec{x} in space. This function is obtained using signed distance transforms, describing the surface S as the zero level set:

$$S = \{ \vec{x} : \phi(\vec{x}) = 0 \}. \quad (1)$$

In order to propagate the surface during an advection step, the level set equation

$$\frac{\partial \phi(\vec{x}, t)}{\partial t} + v(\vec{x}) |\nabla \phi(\vec{x}, t)| = 0 \quad (2)$$

is solved in time t , given the scalar velocity field $v(\vec{x})$ which describes the surface normal velocity at each point. This is achieved by discretizing the level set function on a regular grid and applying a finite difference scheme to solve Eq. (2). The velocity field is generated by extending the calculated surface rates to all points in the simulation space. These surface rates are calculated using surface kinetics models, described in the next section.

2.2. Surface Kinetics

To analyze the surface kinetics which describe the plasma etch process, a model based on the theory of active surface sites is applied [19]. The surface propagation is a result of concurrent etching and deposition phenomena. For this reason, three different types of particle species must be considered:

1. A reactive etchant forming volatile etch products which dissociate thermally and thus etch the substrate;
2. A passivating species which forms protective polymer layers on the surface;

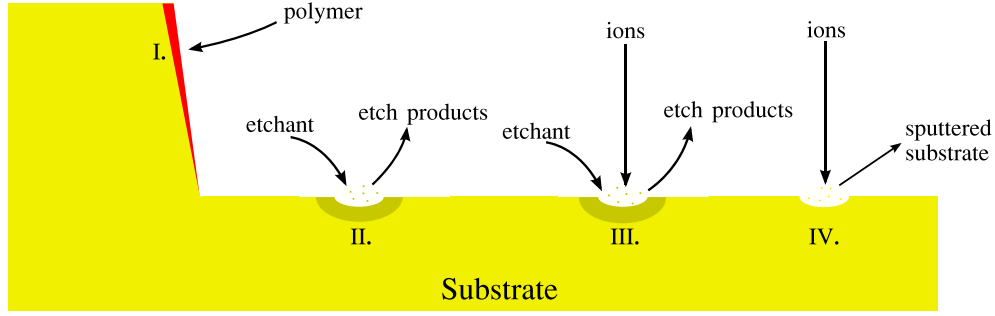


Fig. 3. Schematic representation of the surface processes simulated during the etching process: I. deposition of polymer, forming a passivation layer, II. chemical etching through thermal evaporation, III. ion-enhanced etching, and IV. physical ion sputtering.

3. Energetic ions which physically sputter the film and enhance the dissociation of the volatile etch products. It should be noted that these high energy ions are the primary source of PID in silicon.

The rates of particle types impinging on the surface can be summed to give the coverages θ_x of different particle types at all surface sites, where x represents the etchant (e), polymer (p), or etchant on polymer (pe). Since the etching time is usually much longer than the surface reaction time scales, we can assume that the coverages reach a steady state on the surface. This means that the amount of the different species found at all times can be expressed in terms of constant fluxes J_x . The coverages can therefore be expressed with the following site balance equations [19]:

- Etchant surface sites balance

$$\frac{d\theta_e}{dt} = J_e S_e (1 - \theta_e - \theta_p) - k_{ie} J_i Y_{ie} \theta_e - k_{ev} J_{ev} \theta_e \approx 0; \quad (3)$$

- Polymer sites balance

$$\frac{d\theta_p}{dt} = J_p S_p - J_i Y_p \theta_{pe} \approx 0; \quad (4)$$

- Etchant on polymer surface balance

$$\frac{d\theta_{pe}}{dt} = J_e S_{pe} (1 - \theta_{pe}) - J_i Y_p \theta_{pe} \approx 0. \quad (5)$$

Here, J_x and S_x represent the different particle fluxes and sticking probabilities, respectively. Y_{ie} is the ion-enhanced etching yield for etchant particles, Y_p is the ion-enhanced etching yield on polymer, Y_{sp} gives the physical ion sputtering yield, and k_{ie} and k_{ev} are the stoichiometric factors for ion-enhanced etching and evaporation, respectively, which are determined by the chemical etching reaction. By solving these steady state equations for the coverages, one can determine etch or deposition rates on the surface. If deposition of polymer dominates, the surface normal velocity is positive and is given by

$$v = \frac{1}{\rho_p} (J_p S_p - Y_p J_i \theta_{pe}), \quad (6)$$

where ρ_p is the atomic polymer density. The first term $J_p S_p$ gives the rate of polymer particles reaching and adsorbing on the surface, while the second term $Y_p J_i \theta_{pe}$ describes the removal of polymer by ion-enhanced etching. Together, these terms describe the deposition of polymer material on the surface, which acts as passivation layer for the chemical etching process. If, on the other hand, etching of the substrate dominates, the negative surface velocity of the substrate is given by

$$v = \frac{1}{\rho_m} [J_{ev} \theta_e + J_i Y_{ie} \theta_e + J_i Y_{sp} (1 - \theta_e)], \quad (7)$$

where ρ_m is the atomic density of the etched material and depends on which layer in the stack is being etched. In Eq. (7) each term accounts for a different type of surface reaction. The first term, $J_{ev} \theta_e$, describes the chemical etching process, where etchants bind chemically with the substrate to form volatile etch products which dissolve thermally from the surface. Thus, the evaporation flux J_{ev} is a parameter proportional to the etchant flux J_e and depends on the chemical gas and surface composition and temperature of the etching plasma. It is given by

$$J_{ev} = K e^{-E_a/k_B T} J_e, \quad (8)$$

where K is a process parameter describing the volatility of the chemical etching process, E_a is the activation energy for thermal etching, k_B is the Boltzmann constant, and T is the temperature. The second term in Eq. (7), $J_i Y_{ie} \theta_e$, describes the contribution of ion-enhanced etching. In this surface reaction, volatile etch products which do not dissolve from the surface thermally, absorb energy from impinging ions and consequently dissolve from the surface. Finally, the last term, $J_i Y_{sp} (1 - \theta_e)$, describes physical sputtering of the substrate by highly energetic ions. Since both chemical and ion-enhanced etching involve etchants, they are proportional to the etchant coverage θ_e , while physical ion sputtering takes place directly on the substrate and is thus proportional to the fraction of the surface not covered by the etchant. These different types of processes, leading to a deformation of the surface, are illustrated in Fig. 3. If polymer forms on the top layer which is being etched, only the removal by ion-enhanced etching is considered and the negative surface velocity is again given by Eq. (6), since ion-enhanced etching proceeds on all surfaces, including those covered by the polymer.

Together, Eq. (6) and Eq. (7) describe the temporal evolution of the surface, given the particle fluxes J_x at each location on the etched substrate, which are calculated using MC ray tracing methods.

2.3. Flux Calculation

In order to calculate the particle fluxes, the particle transport moving towards the sample surface inside the etching reactor must be simulated. Since the particle's traversal inside the reactor depends on the specific geometry of the reactor and the processing conditions prevailing inside it, the reactor is divided into reactor-scale and feature-scale regions during simulations, separated by the so-called source plane [20]. The feature-scale region describes the space directly above the wafer, being comparable in size to the geometric features generated by processing the wafer.

The reactor-scale region, on the other hand, is much larger than the feature-scale region and particle transport inside the reactor-scale region is governed by Maxwell-Boltzmann statistics. This is the case, since the reactor-scale region is much larger in comparison to the mean free

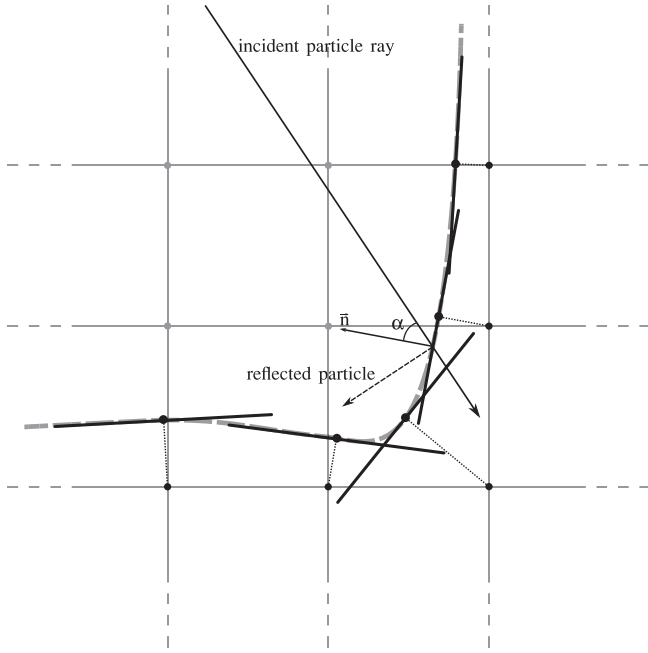


Fig. 4. Schematic representation of a 2D surface using disks. If a particle trajectory intersects any tangential disk, it contributes to the rates of the corresponding grid point. Reflected particles are then traced, starting from the first disk intersection point. Here, reflection of a particle is illustrated with an incidence angle α to the surface normal \vec{n} . We also note that the incident particle ray will intersect with two disks.

path of the particles, which is in the range of 100 μm to 10 mm. The feature scale region, however, is small compared to the mean free path, on the order of a few hundred nm, meaning that collisions with the surface are much more frequent than those with other particles in the gas phase. Therefore, ballistic transport can be used to describe the propagation of particles through the feature scale region, which can be simulated in a straightforward manner using ray tracing methods. In particular, a top-down Monte Carlo ray tracing approach is used, where a large number of particles are launched from a source plane and are traced towards the substrate surface in order to determine the point of impact. Each particle will usually represent several hundred molecules or ions of a particular species which correspond to the particle species described in the previous section, i.e., etchant, polymer, or energetic ions. Since the particles in the feature-scale region are independent of each other, the surface intersection calculations can be parallelized straight-forwardly, which renders this method computationally efficient [21].

For the calculation of the precise location of the surface impact, the implicit surface, given by the level set representation, is converted to an intermediate explicit representation by placing a tangential disc at each surface point [22]. Each disc is angled so that its normal is equal to the surface normal and its radius d_r is determined by the grid spacing d_g . To ensure, the discs form a closed surface with no holes, the disc radius is given by

$$d_r = \frac{\sqrt{3}}{2} d_g. \quad (9)$$

However, this implementation leads to partially overlapping disks and thus intersections can occur on multiple disks. A schematic example of a surface represented by discs, including intersections, is given in Fig. 4.

Particles are first initialized at random positions on the source plane with random directions according to particle-specific distributions. Both polymer and etchant are neutral particles and thus are not affected by the electric sheath potential inside the plasma reactor. Therefore, their

initial directions can be approximated by a simple cosine distribution. Ions, on the other hand, are accelerated towards the surface by the sheath potential. Therefore, their initial distribution is represented with a power cosine distribution, meaning that their movement is more directional towards the surface [23].

The ion yield efficiencies on the point of impact are dependent on the ion energy E , as well as the incident angle α between the ion particle and the surface normal. The initial energy for each ion particle is assigned based on the process used. In general, the ion yield efficiency for physical sputtering and ion-enhanced etching upon impact on the surface can be expressed as

$$Y = A(\sqrt{E} - \sqrt{E_{th}})f(\alpha), \quad (10)$$

where A is a process-dependent constant, describing the particle yield per unit of energy, E_{th} is the minimum energy ions must attain to etch the substrate, referred to as threshold energy, and $f(\alpha)$ is a function of the incident angle. For physical ion sputtering, this function can be approximated using the expression

$$f(\alpha) = (1 + B_{sp}(1 - \cos^2(\alpha)))\cos(\alpha), \quad (11)$$

while for ion-enhanced etching, the expression

$$f(\alpha) = \cos(\alpha) \quad (12)$$

is applied, as described in [19].

If the energy of an ion is below the threshold, it is reflected specularly, until it reaches a point with a larger incident angle or until it leaves the simulation domain. The ion energy is however adjusted at each surface reflection according to the angle-dependent yield efficiencies.

Polymer and etchant particles, on the other hand, reflect diffusely from the surface. A weight factor which describes the probability of the particle taking the modeled trajectory is reduced after each reflection with particle dependent sticking probabilities. The particles are tracked until the weight factor drops below a certain limit or the particle leaves the simulation domain.

2.4. Plasma Impact Damage

In HAR etching processes, the use of high energy ions in a plasma is necessary to achieve the desired channel aspect ratios. However, this introduces the problem of high energy ions being able to penetrate into the bottom substrate, consequently leading to a disordered silicon layer on the bottom of the channel hole, thereby destroying the crystal purity. Experimental studies of ion induced etching damage show that the damaged layer is composed of impurities related to the etchant chemistry [15,24]. To model this damaged layer in the crystalline silicon substrate, the energy of traced ions is recorded on the substrate surface at each flux calculation step. Since the highest ion energies occur at normal incidence, the recorded energies can be applied to model the ion damage in the material directly below the surface. At each surface point, the impinging ion energy E is assumed to decrease through the substrate due to scattering off the silicon atoms, following an exponential attenuation given by

$$E(d) = E_i e^{-d/\lambda}, \quad (13)$$

where E_i is the initial ion energy upon surface impact and d is the normal distance to the surface inside the material, equivalent to the penetration depth. Given the observed thickness of the damaged layer $d_{th} = 8$ nm, as noted in Fig. 2 [14], and the threshold energy for ion-enhanced etching E_{th} , the attenuation length λ is determined as

$$\lambda = d_{th} / \ln\left(\frac{E_i}{E_{th}}\right). \quad (14)$$

Subsequently, an ion damage coefficient $D(d)$ is defined and stored for

each surface point of the geometry. The coefficient is proportional to the ion energy at a depth d in the substrate:

$$D(d) \propto E(d) - E_{th}. \quad (15)$$

In order for silicon to grow epitaxially, the material must not be damaged and hence, the ion damage coefficient at the surface must fulfill $D \leq 0$ for growth to take place, which equivalently describes $E(d) \leq E_{th}$. To remove the damaged layer in a post etch treatment process, the surface is etched using low energy ions [14]. Assuming these low energy ions do not cause any additional implantations in the substrate, the surface is etched until the damage coefficient D at the bottom drops below 0, thereby forming a suitable highly crystalline interface for the subsequent selective epitaxial growth.

The surface damage coefficient D is stored as a local parameter at each surface point on the surface level set. During the surface propagation in the post etch treatment, the damage coefficient is reduced according to the exponential attenuation given in Eq. (15), where d is the advected distance in the direction of the surface normal. In order to accurately transport the damage coefficient to the new surface after each advection step, we use the Manhattan normalization. First, we assume that along a surface normal all local surface properties remain unaltered. From the level set equation, we know that information only propagates along the surface normal and thus every new grid point acquires the properties from the grid point from which it arises. Similar to level set advection, this method is very accurate if the surface propagates along its grid lines, but less accurate if it moves diagonal to its grid lines.

2.5. Selective Epitaxial Growth

For the simulation of SEG, the specialized numerical method presented by Toifl et al. [17] is applied. In this approach the numerical integration of the level set equation is enhanced by introducing numerical dissipation coefficients based on the Stencil Lax-Friedrichs flux [25], which ensure a monotonic and thus stable evolution of the surface. The rates for the velocity function, which describe the surface evolution are extracted from experimental studies, as described in Section 3.2. The scheme does not rely on numerical calibration parameters and can therefore be employed for generic velocity functions which are purely surface normal-dependent. Additionally, the level set advection is carried out on an additional deposition top layer to robustly handle multiple material regions.

In the SEG step, the algorithm is applied at all surface points describing the bottom Si layer, where the surface damage coefficient fulfills $D \leq 0$. This way it is ensured that SEG commences only on a crystalline Si surface.

3. Process Chemistry

3.1. Plasma Etching

Etching is modeled in a fluorocarbon based etch process, including Ar and O₂ as inhibitor, as is commonly used for the etching of SiO₂/Si₃N₄ layers [26]. As described in Section 2.2, three different physical processes lead to the etching of a substrate: Chemical etching, ion-enhanced etching, and physical sputtering. Fluoride reacting chemically with the silicon surfaces leads to etch products which evaporate back in the gas phase [27]. The fluorocarbon radicals CF_x⁺ together with Ar⁺ provide ion bombardment which enables ion-enhanced etching and physical sputtering, where etch products evaporate from the surface due to their now smaller binding energies, or as a result of receiving momentum from the collision cascade induced by the incident ion [28]. The threshold energy E_{th} for physical sputtering is related to the binding energy of the substrate. The addition of O₂ enables the formation of a passivation layer on the sidewall of the substrate, which inhibits lateral etching. The parameters describing these processes in the etching model

Table 1

Parameters used for the simulation of the vertical channel hole etching process. Values are extracted from [19,29].

Parameter	Value	Description
J_{ion}^{src}	$1 \times 10^{17} \text{ cm}^{-2} \text{ s}^{-1}$	Source ion flux
J_{etch}^{src}	$5 \times 10^{17} \text{ cm}^{-2} \text{ s}^{-1}$	Source etchant flux
J_{poly}^{src}	$1 \times 10^{17} \text{ cm}^{-2} \text{ s}^{-1}$	Source polymer flux
A_{sp}	$0.00339 \text{ eV}^{-1/2}$	Yield coefficient in (10) for physical ion sputtering
A_{ie}^e	$0.0361 \text{ eV}^{-1/2}$	Yield coefficient in (10) for ion-enhanced etching (substrate)
A_{ie}^p	$4A_{ie}^e$	Yield coefficient in (10) for ion-enhanced etching (polymer)
B_{sp}	9.3	Sputtering yield angular factor in (11)
E_{sp}^{th}	18 eV	E_{th} for physical ion sputtering
$E_{ie,e}^{th}$	4 eV	E_{th} for ion-enhanced etching (substrate)
$E_{ie,p}^{th}$	4 eV	E_{th} for ion-enhanced etching (polymer)
E_{ion}	100 eV	Mean initial ion energy
E_a	0.168 eV	Activation energy in (8)
k_{ie}, k_{ev}	1	Stoichiometric factors
S_e	0.9	Etchant particle sticking probability
S_p	0.26	Polymer particle sticking probability
S_{pe}	0.6	Etchant on polymer sticking probability
K	$2.7 \times 10^{-3} \text{ cm}^{-2} \text{ s}^{-1}$	Volatility parameter in evaporation flux (8)
T	300 K	Temperature
ρ_{SiO_2}	$2.2 \times 10^{22} \text{ cm}^{-3}$	SiO ₂ density
$\rho_{Si_3N_4}$	$10.3 \times 10^{22} \text{ cm}^{-3}$	Si ₃ N ₄ density
ρ_{Si}	$5.02 \times 10^{22} \text{ cm}^{-3}$	Si density
ρ_p	$2.0 \times 10^{22} \text{ cm}^{-3}$	Polymer density

Table 2

Parameters used for the simulation of the post etch treatment process, which differ from those in the vertical etching process and parameters to model the ion damage.

Parameter	Value	Description
S_e	0.1	Etchant particle sticking probability
E_{ion}	10 eV	Mean initial ion energy
E_{th}	4 eV	Threshold energy for ion damage to occur
d_{th}	8 nm	Depth of the damaged layer as observed in [14]

are extracted from [19,29] and summarized in Table 1. For simplicity, the ion energies are randomly initialized based on a Gaussian distribution around an initial mean energy E_{ion} corresponding to the sheath potential, approximating the results for inductively coupled plasma chemistries from [30].

For the post etch treatment, Luo et al. proposed a chemistry based on an inductively coupled plasma using low energy Cl₂ and NF₃/CH₂F₂ gases [14]. By lowering the plasma energy, chemical etching dominates the etching process and ions do not penetrate deep into the surface as is the case with the first etch step. The basic etch mechanisms, however, are the same as in fluorocarbon plasmas. Thus, we can reuse the surface kinetic model with adjusted parameters. In order to account for Cl₂ plasma, the sticking probability for etchant particles is set to the corresponding values for Cl₂. The initial ion energy is lowered, while the initial particle fluxes for ions and neutral particles are kept the same. The parameters which are different to the fluorocarbon plasma are summarized in Table 2.

3.2. Selective Epitaxial Growth

During selective epitaxial growth, silicon is grown on a clean crystalline silicon surface, through the adsorption from Si atoms from the gas phase. On the microscopic scale epitaxial growth is governed by the movement of individual atoms mainly through adsorption, surface diffusion, nucleation, and film coalescence [31]. For a continuum model of epitaxy, the atomistic nature of matter is neglected and microscopic

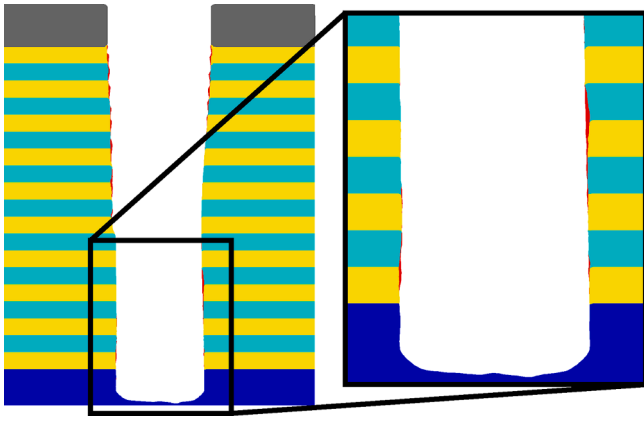


Fig. 5. Final 2D profile slice of the HAR hole etching simulation. The alternating $\text{SiO}_2/\text{Si}_3\text{N}_4$ layers (yellow/cyan) are etched down to a bottom Si layer (blue). The thin sidewall layers (red) represent the deposited polymer formed during the etching process.

processes are abstracted with distributed quantities and material properties. Since the incoming atom flux is determined by a single neutral particle species, the flux is assumed to follow Knudsen diffusion in the hole and is thus independent of the lateral position on the wafer. For this reason, the incoming atom flux and incorporation can be represented by growth rates which depend only on the crystal orientation and growth conditions. Growth rates of crystal facets can be experimentally characterized through techniques such as atomic force microscopy (AFM) or cross-sectional transmission electron microscopy (TEM). Therefore, an empirical growth rate function which provides the growth rate of all crystal orientations is constructed. The corresponding rates are extracted from experimental studies by Dutartre et al. [32].

4. Simulation Setup

The structure of the simulation domain is based on the multi-material representation presented by Ertl and Selberherr [33]. In this approach, the stacked material layers are represented using individual level sets which are connected by sequential union operations. This multi-material representation enables the resolution of thin layer regions (i.e., thickness below a single grid spacing) and thus an additional layer, placed on top of all layers, is used to capture any deposited polymer.

The geometry of the 60 nm diameter hole is resolved on a regular grid with lateral extensions 64×64 and a grid spacing of 1.5 nm. Reflective boundary conditions are assumed in both lateral directions. The etching simulation and post etch treatment process each consist of multiple steps of alternating ray tracing and surface advection. In the ray tracing step, the required fluxes at each surface point are calculated and used to find the resulting surface velocity which is applied for the subsequent level set advection step. The advection step solves the level set equations and moves the surface, effectively identifying the new location of the surface. In the advection algorithm, the time-discretization Δt is adjusted to the previously calculated rates. The algorithm determines the maximum time step possible, according to the Courant-Friedrichs-Lewy (CFL) condition [34] for a sparse level set [22]

$$\max|\phi(\vec{x}, t + \Delta t) - \phi(\vec{x}, t)| \leq 0.5. \quad (17)$$

This ensures a stable time integration during level set advection.

The number of rays traced is also adjusted during the evolution of the surface. For each grid point a minimum of 3000 rays is simulated to ensure a statistically converged result. This results in anywhere between 3 and 11 million trajectories of each particle species being calculated during each time step. For this reason the main plasma etching simulation was performed on a 40-core Intel Xeon Gold node of a cluster with



Fig. 6. Clipped 3D surface representation of the ion damage (a) prior to the post etch treatment, and (b) after the post etch treatment.

a computation time of about 2 h. The simulation of the post-etch treatment and the subsequent SEG was carried out on a single workstation with an Intel i7-3770 CPU, requiring approximately 15 min.

5. Results

5.1. Vertical Channel Hole Etching

The geometric profile of the stacked sheets after the etching simulation is shown in Fig. 5. The etch process is performed until the hole is slightly over-etched in the bottom silicon substrate. On the sidewall one can observe the thin passivation layer in red, formed during the etching process.

The damage coefficient on a 3D clip of the surface after the etching process is shown in Fig. 6. Due to the high directional trajectories of ions and the angle-dependent etching yield, the resulting ion damage is predominately confined to the bottom regions of the trench, which is also confirmed experimentally in [14].

An additional effect caused by energetic ions is the charging of dielectric materials, as reported by Memos et al. [35]. The charging of $\text{SiO}_2/\text{Si}_3\text{N}_4$ layers could lead to small non-spectral deflections of the ion trajectories and could affect the etching profile [36,37]. However, most of the damage recorded on the bottom surface is caused by energetic ions which directly hit the surface and are not reflected from the sidewalls. The particles which do reflect off the sidewalls and still have enough energy to damage the crystalline substrate must reflect at very high angles to the surface normal. This results in highly specular reflections with only a minimal loss of energy, as is assumed in our reflection model. Therefore, the surface charging effect on the sidewall is not expected to have a large impact on the ion damage recorded at the

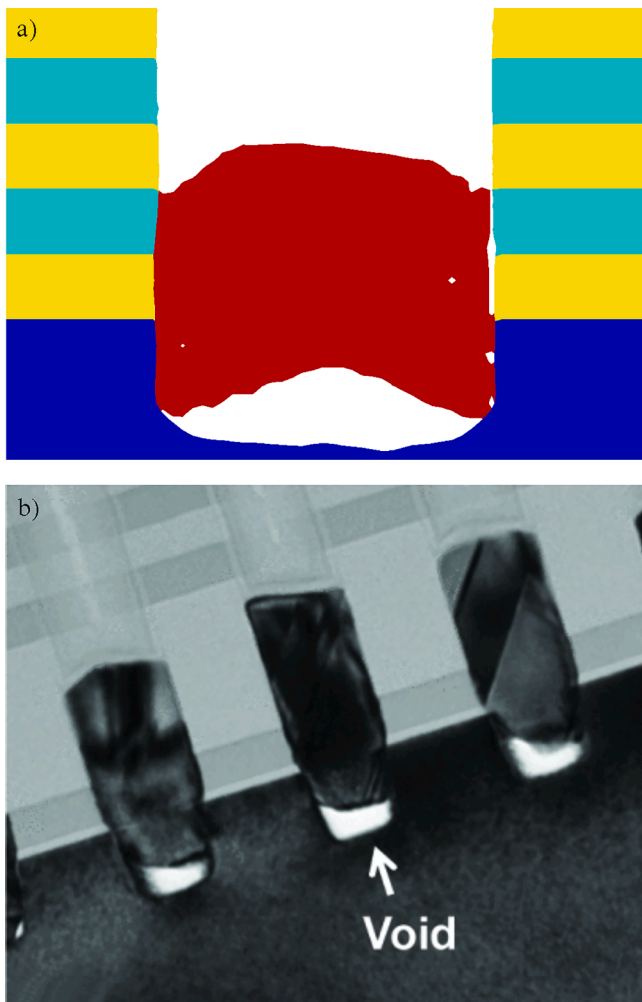


Fig. 7. (a) Results of the selective epitaxial growth of silicon (red) after the etching process without post etch treatment, on the bottom of a cropped 2D slice of the trench. The damaged layer on the surface is covering parts of the Si layer (blue), hence leading to an ill-formed SEG. (b) A similar behavior is observed in the experimental findings by Lung et al. [15] (@ 2019 IEEE. Reprinted, with permission from C.-Y. Lung et al., "Pre-epitaxial plasma etch treatment for the selective epitaxial growth of silicon in high aspect ratio 3D NAND memory", in: 30th Annual SEMI Advanced Semiconductor Manufacturing Conference (ASMC), 2019 [15]).

bottom. However, some charging can also take place at the bottom of the hole, ultimately resulting in a reduction in the impacting ion energy and in the surface etch rate, an effect which was excluded in this study. Nevertheless, the implemented model provides for the flexibility of including any additional effects, specifically because the surface charge can be stored as a parameter within the framework, similar to the way that the damage parameter is stored. For this, only Eq. (10) would need to be adapted to include the effects of surface charging.

During the post-etch treatment, the surface is etched with low energy ions, until the damaged layer has been removed and the crystalline silicon material underneath is revealed, in order for the SEG step to commence on a pure crystal surface. During the surface propagation in the post etch treatment, the damage coefficient is reduced according to the exponential attenuation given in Eq. (15), where d is the advected distance in the direction of the surface normal.

5.2. Selective Epitaxial Growth of Silicon

Next, selective epitaxial growth of silicon at the bottom of the channel hole is carried out on the final profile after the post etch

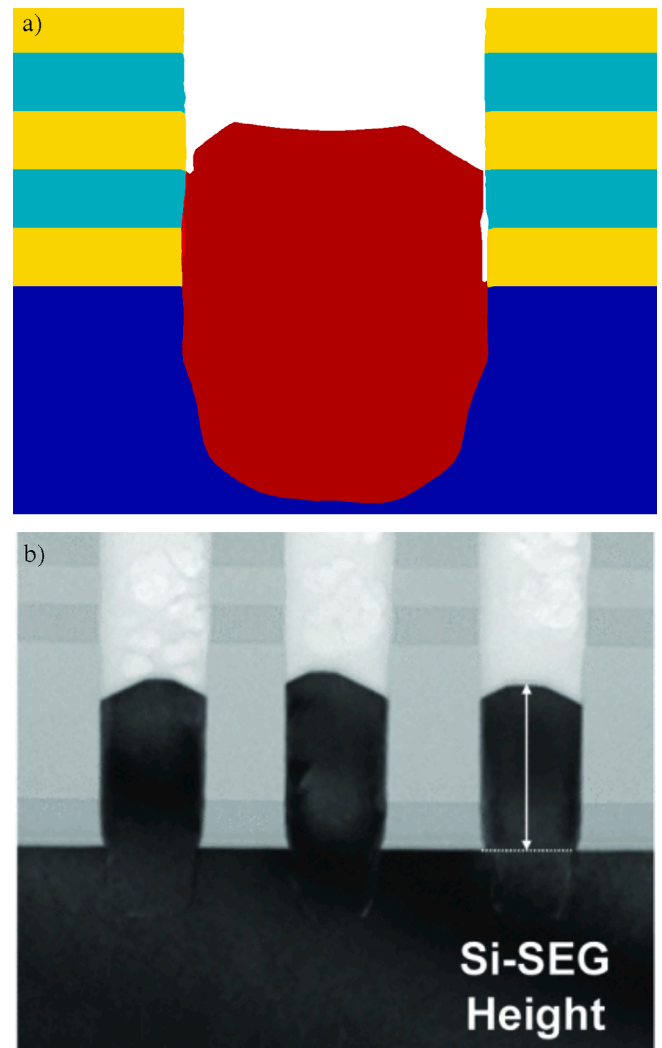


Fig. 8. Figure a shows the results for the selective epitaxial growth of silicon (red) after the etching process, on the bottom of a cropped 2D slice of the trench. The damaged layer has been removed in a post etch treatment and the SEG covers the entire bottom, leaving no voids. (b) Experimental findings by Lung et al. [15] depict a similar result (@ 2019 IEEE. Reprinted, with permission from C.-Y. Lung et al., "Pre-epitaxial plasma etch treatment for the selective epitaxial growth of silicon in high aspect ratio 3D NAND memory", in: 30th Annual SEMI Advanced Semiconductor Manufacturing Conference (ASMC), 2019 [15]).

treatment. When the damaged layer is present on the silicon substrate a large void is observed, as shown in Fig. 7. Since the disordered layer covers most of the bottom, as observed in Fig. 6, there are only certain points on the sidewall, where SEG can initiate. Such voids lead to an ill-formed contact to the silicon source line, which will heavily impact the bottom select gate characteristics and reduce the overall quality of the memory stack.

However, when the silicon substrate is cleaned prior to SEG, as described in the previous section, the desired SEG growth is obtained with the grown layer providing full contact with the silicon source line, as can be seen in Fig. 8. The simulation results can be qualitatively compared to the experimental results observed by Lung et al. [15], showing the TEM images of the final structure after SEG with and without a post-etch treatment to clean the silicon substrate, respectively.

6. Conclusion

A physical process model is applied to simulate vertical channel hole

etching in sequential SiO₂/Si₃N₄ 3D NAND flash memory stacks. The model, based on a level set surface representation and Monte Carlo ray tracing for flux calculation, is able to simulate the damage induced in a crystalline silicon substrate by ion-enhanced etching. The damage caused on the bottom silicon substrate is modeled using a surface damage coefficient, relating the etch damage to the relative position on the surface using an ion penetration depth. Subsequent silicon SEG is shown to form undesired voids with the damaged layer present, similar to experimental findings [15]. In a pre-epitaxial post etch treatment process, the damaged substrate is removed by low energy ions until the crystalline silicon at the bottom is exposed. The subsequent SEG of silicon provides full contact with the source line, leaving no undesirable voids. This is modeled using the surface damage coefficient which is decreased according to an exponential attenuation, during the etching of the bottom substrate. Due to the physical nature of the presented model, relevant physical effects and underlying etch mechanisms are represented appropriately. Therefore, the proposed model allows to analyze the physical behavior of the etch process in order to optimize the fabrication conditions during channel hole etching and the post etch treatment fabrication steps. Hence, the model serves as a basis for an enhanced understanding of source contact formation in 3D NAND memory cells.

The broad applicability of the developed tools to deal with topography and volume problems provides a sound basis for future studies in damage induced effects during etching processes and other detrimental phenomena taking place during fabrication. The ability to store and process surface information during the simulation of a sequence of fabrication steps allows for the analysis of the impact of damage in various regions of the modeled device.

Declaration of Competing Interest

The authors declare that they have no known competing financial interests or personal relationships that could have appeared to influence the work reported in this paper.

Acknowledgment

This work was supported in part by the Austrian Research Promotion Agency FFG (Bridge Young Scientists) under Project 878662 "Process-Aware Structure Emulation for Device-Technology Co-Optimization".

The authors acknowledge TU Wien Bibliothek for financial support through its Open Access Funding Programme.

References

- [1] Fukuzumi Y, Katsumata R, Kito M, Kido M, Sato M, Tanaka H, et al. Optimal integration and characteristics of vertical array devices for ultra-high density, bit-cost scalable flash memory. 2007 IEEE International Electron Devices Meeting. Washington DC, USA: IEEE; 2007. p. 449–52. <https://doi.org/10.1109/IEDM.2007.4418970>.
- [2] Tanaka H, Kido M, Yahashi K, Oomura M, Katsumata R, Kito M, et al. Bit cost scalable technology with punch and plug process for ultra high density flash memory. In: 2007 IEEE Symposium on VLSI Technology. Kyoto, Japan: IEEE; 2007. p. 14–5. <https://doi.org/10.1109/VLSIT.2007.4339708>.
- [3] Li Y. 3D NAND memory and its application in solid-state drives: Architecture, reliability, flash management techniques, and current trends. IEEE Solid-State Circuits Mag. 2020;12(4):56–65. <https://doi.org/10.1109/MSSC.2020.3021841>.
- [4] Kim H, Ahn S-J, Shin YG, Lee K, Jung E. Evolution of NAND flash memory: From 2D to 3D as a storage market leader. 2017 IEEE International Memory Workshop (IMW). Monterey, CA, USA: IEEE; 2017. p. 1–4. <https://doi.org/10.1109/IMW.2017.7939081>.
- [5] Bassett D, Printz W, Furukawa T. Etching of silicon nitride in 3D NAND structures. ECS Trans 2015;69(8):159–67. <https://doi.org/10.1149/06908.0159ecst>.
- [6] Lapedus M. 3D NAND's vertical scaling race, Semiconductor Engineering 2020; URL: <https://semiengineering.com/3d-nands-vertical-scaling-race/>.
- [7] Oehrlein GS. Dry etching damage of silicon: A review. Mater Sci Eng: B 1989;4(1–4):441–50. [https://doi.org/10.1016/0921-5107\(89\)90284-5](https://doi.org/10.1016/0921-5107(89)90284-5).
- [8] Martin A. Review on the reliability characterization of plasma-induced damage. J Vacuum Sci Technol B 2009;27(1):426–34. <https://doi.org/10.1116/1.3054356>.

- [9] Eriguchi K. Defect generation in electronic devices under plasma exposure: Plasma-induced damage. Jpn J Appl Phys 2017;56(6S2):06HA01-1-06HA01-21. <https://doi.org/10.7567/JJAP.56.06HA01>.
- [10] Eriguchi K, Ono K. Quantitative and comparative characterizations of plasma process-induced damage in advanced metal-oxide-semiconductor devices. J Phys D 2008;41(2):024002-1–024002-10. <https://doi.org/10.1088/0022-3727/41/2/024002>.
- [11] Yabumoto N, Oshima M, Michikami O, Yoshii S. Surface damage on Si substrates caused by reactive sputter etching. Jpn J Appl Phys 1981;20(5):893–900. <https://doi.org/10.1143/JJAP.20.893>.
- [12] Cheung KP, Chang CP. Plasma-charging damage: A physical model. J Appl Phys 1994;75(9):4415–26. <https://doi.org/10.1063/1.355985>.
- [13] Yunogami T, Mizutani T, Suzuki K, Nishimatsu S. Radiation damage in SiO₂/Si induced by VUV photons. Jpn J Appl Phys 1989;28(Part 1, No. 10):2172–6. <https://doi.org/10.1143/JJAP.28.2172>.
- [14] Luo L, Lu Z, Zuo X, Zhang Y, Zhang B, Zhao C, et al. An effective process to remove etch damage prior to selective epitaxial growth in 3D NAND flash memory. Semicond Sci Technol 2019;34(9):095004-1–095004-5. <https://doi.org/10.1088/1361-6641/ab3130>.
- [15] Lung C-Y, Chung Y-A, Wu M-T, Lee H-J, Lian N-T, Yang T, et al. Pre-epitaxial plasma etch treatment for the selective epitaxial growth of silicon in high aspect ratio 3D NAND memory. 2019 30th Annual SEMI Advanced Semiconductor Manufacturing Conference (ASMC). Saratoga Springs, NY, USA: IEEE; 2019. p. 1–5. <https://doi.org/10.1109/ASMC.2019.8791765>.
- [16] Klemenschits X et al., ViennaTools (Sep. 2021). URL: <https://github.com/ViennaTools>.
- [17] Toifl A, Quell M, Klemenschits X, Manstetten P, Hossinger A, Selberherr S, Weinbub J. The level-set method for multi-material wet etching and non-planar selective epitaxy. IEEE Access 2020;8:115406–22. <https://doi.org/10.1109/ACCESS.2020.3004136>.
- [18] Sethian JA. Level Set Methods and Fast Marching Methods: Evolving Interfaces in Computational Geometry, Fluid Mechanics, Computer Vision, and Materials Science. 2nd. Cambridge University Press; 1999.
- [19] Magna AL, Garozzo G. Factors affecting profile evolution in plasma etching of SiO₂. J Electrochem Soc 2003;150(10):F178–85. <https://doi.org/10.1149/1.1602084>.
- [20] Klemenschits X, Selberherr S, Filipovic L. Modeling of gate stack patterning for advanced technology nodes: A review. Micromachines 2018;9(12):631-1–631-31. <https://doi.org/10.3390/mi9120631>.
- [21] Filipovic L, Ertl O, Selberherr S. Parallelization strategy for hierarchical run length encoded data structures, in: Proceedings of the IASTED International Conference on Parallel and Distributed Computing and Networks (PDCN); 2011. p. 131–8. <https://doi.org/10.2316/P.2011.719-045>.
- [22] Ertl O, Selberherr S. Three-dimensional level set based bosch process simulations using ray tracing for flux calculation. Microelectron Eng 2010;87(1):20–9. <https://doi.org/10.1016/j.mee.2009.05.011>.
- [23] Plummer JD, Deal M, Griffin PB. Silicon VLSI Technology. 2nd Edition. USA: Prentice Hall Press; 2008.
- [24] Nakahata T, Yamamoto K, Tanimura J, Inagaki T, Furukawa T, Maruno S, Tokuda Y, Miyamoto A, Satoh S, Kiyama H. Low thermal budget surface cleaning after dry etching for selective silicon epitaxial growth. J Cryst Growth 2001;226(4):443–50. [https://doi.org/10.1016/S0022-0248\(01\)01407-5](https://doi.org/10.1016/S0022-0248(01)01407-5).
- [25] Osher S, Fedkiw, R. Level Set Methods and Dynamic Implicit Surfaces, Vol. 153 of Applied Mathematical Sciences, Springer New York, New York, NY, 2003. <https://doi.org/10.1007/b98879>.
- [26] Iwase T, Matsui M, Yokogawa K, Arase T, Mori M. Role of surface-reaction layer in HBr/fluorocarbon-based plasma with nitrogen addition formed by high-aspect-ratio etching of polycrystalline silicon and SiO₂ stacks. Jpn J Appl Phys 2016;55(6S2):06HB02-1–5. <https://doi.org/10.7567/JJAP.55.06HB02>.
- [27] Mauer JL, Logan JS, Zielinski LB, Schwartz GC. Mechanism of silicon etching by a CF₄ plasma. J Vacuum Sci Technol 1978;15(5):1734–8. <https://doi.org/10.1116/1.569836>.
- [28] Tu Y-Y, Chuang TJ, Winters HF. Chemical sputtering of fluorinated silicon. Phys Rev B 1981;23(2):823–35. <https://doi.org/10.1103/PhysRevB.23.823>.
- [29] Gogolides E, Vauvert P, Kokkoris G, Turban G, Boudouvis AG. Etching of SiO₂ and Si in fluorocarbon plasmas: A detailed surface model accounting for etching and deposition. J Appl Phys 2000;88(10):5570–84. <https://doi.org/10.1063/1.1311808>.
- [30] Belen RJ, Gomez S, Kiehlbauch M, Cooperberg D, Aydil ES. Feature-scale model of Si etching in SF₆ plasma and comparison with experiments. J Vacuum Sci Technol A 2005;23(1):99–113. <https://doi.org/10.1116/1.1830495>.
- [31] Pohl UW. Epitaxy of Semiconductors: Physics and Fabrication of Heterostructures, Graduate Texts in Physics. Springer International Publishing 2020. <https://doi.org/10.1007/978-3-030-43869-2>.
- [32] Dutarré D, Talbot A, Loubet N. Facet propagation in Si and SiGe epitaxy or etching. ECS Trans 2019;3(7):473–87. <https://doi.org/10.1149/1.2355845>.
- [33] Ertl O, Selberherr S. A fast level set framework for large three-dimensional topography simulations. Comput Phys Commun 2009;180(8):1242–50. <https://doi.org/10.1016/j.cpc.2009.02.002>.
- [34] Courant R, Friedrichs K, Lewy H. Über die partiellen Differenzgleichungen der mathematischen Physik. Math Ann 1928;100(1):32–74. <https://doi.org/10.1007/BF01448839>.

- [35] Memos G, Kokkoris G. Modeling of charging on unconventional surface morphologies of PMMA substrates during Ar plasma etching. *Plasma Processes Polym* 2016;13(5):565–78. <https://doi.org/10.1002/ppap.201500176>.
- [36] Memos G, Lidorikis E, Kokkoris G. The interplay between surface charging and microscale roughness during plasma etching of polymeric substrates. *J Appl Phys* 2018;123(7):073303-1–073303-9. <https://doi.org/10.1063/1.5018313>.
- [37] Memos G, Lidorikis E, Kokkoris G. Roughness evolution and charging in plasma-based surface engineering of polymeric substrates: The effects of ion reflection and secondary electron emission. *Micromachines* 2018;9(8):415-1–415–416. <https://doi.org/10.3390/mi9080415>.



Tobias Reiter was born 1996 in Steyr, Austria. He received his Bachelor's degree in Technical Physics in 2019 and is now enrolled in the Master's Program Technical Physics, as well as the Master's Program Computational Science and Engineering, both at TU Wien, Austria. In 2021 he joined the Institute for Microelectronics, where his main research focus is the development of a process simulation framework for semiconductor device fabrication.